In situ measurements and modeling of reactive trace gases in a small biomass burning plume

M. Müller[1,2], B. Anderson[3], A. Beyersdorf[3], J. H. Crawford[3], G. Diskin[3], P. Eichler[1], A. Fried[4], F. N. Keutsch[5,] T. Mikoviny[6], K. L. Thornhill[3,7], J. G. Walega[4], A. J. Weinheimer[8], M. Yang[3], R. Yokelson[2], and A. Wisthaler[1,6]

[1]{Institute of Ion Physics and Applied Physics, University of Innsbruck, Innsbruck, Austria}

[2]{Department of Chemistry, University of Montana, Missoula, MT, USA}

[3]{NASA Langley Research Center, Hampton, Virginia, USA}

[4] {Institute of Arctic and Alpine Research, University of Colorado, Boulder, CO, USA}

[5]{School of Engineering and Applied Sciences, Department of Chemistry and Chemical Biology Harvard University, Cambridge, MA, USA}

[6]{Department of Chemistry, University of Oslo, Oslo, Norway}

[7]{Science Systems and Applications, Inc., Hampton, Virginia, USA}

[8]{Atmospheric Chemistry Observations and Modeling Laboratory, National Center for Atmospheric Research, Boulder, CO, USA}

Correspondence to: A. Wisthaler (armin.wisthaler@uibk.ac.at)

Abstract

An instrumented NASA P-3B aircraft was used for airborne sampling of trace gases in a plume that had emanated from a small forest understory fire in Georgia, USA. The plume was sampled at its origin for deriving emission factors and followed ~ 13.6 km downwind for observing chemical changes during the first hour of atmospheric aging. The P-3B payload included a proton-transfer-reaction time-of-flight mass spectrometer (PTR-ToF-MS), which measured non-methane organic gases (NMOGs) at unprecedented spatio-temporal resolution (10m/0.1s). Quantitative emission data are reported for CO_2, CO, NO, NO_2, HONO, NH_3 and 16 NMOGs (formaldehyde, methanol, acetonitrile, propene, acetaldehyde, formic acid, acetone plus its isomer propanal, acetic acid plus its isomer glycolaldehyde, furan, isoprene plus isomeric pentadienes and cyclopentene, methyl vinyl ketone plus its isomers crotonaldehyde and methacrolein, methylglyoxal, hydroxy acetone plus its isomers methyl acetate and propionic acid, benzene, 2,3-butandione and 2-furfural) with molar emission ratios relative to CO larger than 1 ppbV $ppmV^{-1}$. Formaldehyde, acetaldehyde, 2-furfural and methanol dominated NMOG emissions. No NMOGs with more than 10 carbon atoms were observed at mixing ratios larger than 50 pptV per ppmV CO emitted. Downwind plume chemistry was investigated using the observations and a 0-D photochemical box model simulation. The model was run on a near-explicit chemical mechanism (MCM v3.3) and initialized with measured emission data. Ozone formation during the first hour of atmospheric aging was well captured by the model, with carbonyls (formaldehyde, acetaldehyde, 2,3-butanedione, methylglyoxal, 2-furfural) in addition to CO and CH_4 being the main drivers of peroxy radical chemistry. The model also accurately reproduced the sequestration of NO_x into PAN and the OH-initiated degradation of furan and 2-furfural at an average OH concentration of 7.45±1.07 $x10^6$ cm^{-3} in the plume. Formaldehyde, acetone/propanal, acetic acid/glycolaldehyde and maleic acid/maleic anhydride (tentatively identified) were found to be the main NMOGs to increase during one hour of atmospheric plume processing, with the model being unable to capture the observed increase. A mass balance analysis suggests that about 50% of the aerosol mass formed in the downwind plume is organic in nature.

1 Introduction

Understanding and predicting the impacts of biomass burning emissions on air quality is a challenging but important task. Fire emissions include a plethora of inorganic and organic species, both in the gas and the particulate phase, and many of them undergo rapid chemical transformations and phase changes after their release to the atmosphere (e.g. Simoneit, 2002). These processes are the focus of intense research efforts, both in the laboratory and in the field. Over the last decade, many airborne field studies have been undertaken for characterizing emissions and evolution of gases and particles in the aging plume (e.g. Akagi et al., 2012, 2013; Yokelson et al., 2009). In general, these studies have targeted emissions from medium and large-scale fires. Small fires (< 500 m diameter of burned area) have been undersampled although they may contribute 35% or more to global biomass burning carbon emissions (Randerson et al., 2012). Emissions from small fires are often not included in emission inventories and local and regional air quality assessments seldom include emissions from small fires. In addition, the chemical complexity of emissions poses a major challenge to modeling efforts. Lumped mechanisms are thus typically used in chemical models to predict the evolution of trace gases in biomass burning plumes. Lumping of species may, however, result in an oversimplification of the involved chemistry, which will ultimately yield erroneous model predictions.

In this work, we present the results from an airborne study, in which inorganic and organic trace gases emanating from a small forest understory fire were measured with state-of-the-art analytical tools. A proton-transfer-reaction time-of-flight mass spectrometry (PTR-ToF-MS) instrument delivered non-methane organic gas (NMOG) data at unprecedented spatio-temporal resolution. We sampled the plume at its origin for deriving emission factors and followed it downwind for observing chemical changes during the first hour of atmospheric aging. We also found that a 0-D photochemical box model, run on a near-explicit chemical mechanism and properly initialized with the measured emission data, adequately described key chemical processes (ozone and radical formation, NOx sequestration) in the aging plume.

2 Methods

2.1 Sampling strategy and conditions

A small biomass burning plume was intercepted by the NASA P-3B research aircraft in Laurens County near Dublin, GA, USA on September 29th, 2013, during a flight from Houston, TX, to Wallops Island, VA. The plume emanated from a managed forest understory fire located at 32° 23' 42" N and 82° 51' 7.2" W which had been applied after logging and forest clearance activities. Historic Google Earth imagery shows that the area to the SW of the fire location had undergone intense forest clearing between 2011 and 2014. After the flight, the burned area was inspected by a local official who identified residual tree logs (pine, oak) and weeds as fire fuels. Figures 1a and 1b are two frames from the P-3B front camera showing the fire and the emanating plume at 17:33:32 UTC (UTC = local time + 4 hours) and 17:42:51 UTC, respectively.

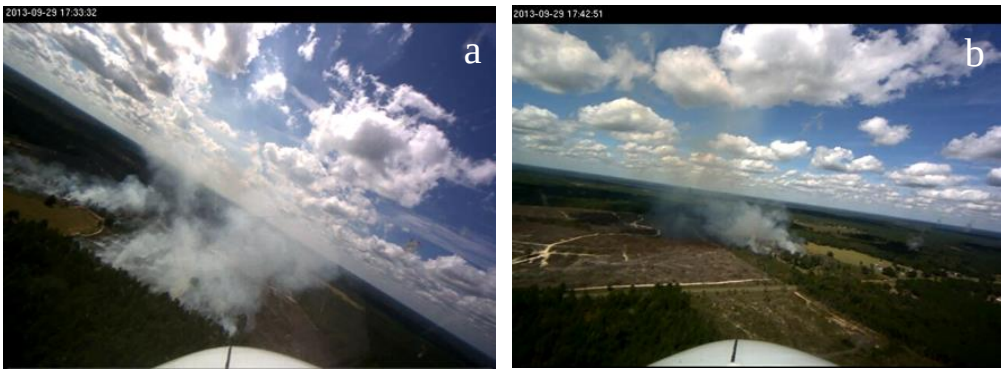

Figure 1. NASA P-3B front camera frames showing the forest understory fire and the emanating biomass burning plume at 17:33:32 (a) and UTC 17:42:51 (b), respectively.

Figure 2 depicts the P-3B flight pattern color-coded in radar altitude, with blue lowest and red highest. The flight direction is indicated by black arrows. Winds steadily blew from the NE at an average speed of 3.5 ms^{-1} (Figure 2, wind rose inset in the upper left corner). The average temperature during the sampling period (17:30-17:55 UTC) as measured by the P-3B met sensors was 26.5 ± 5.3 °C and the average relative humidity was 60.4 ± 2.3 %. The average vertical temperature gradient was -1.34 °C/100 m, causing the plume to slowly rise downwind of the source. The turbulence condition of the boundary layer was neutral to slightly unstable.

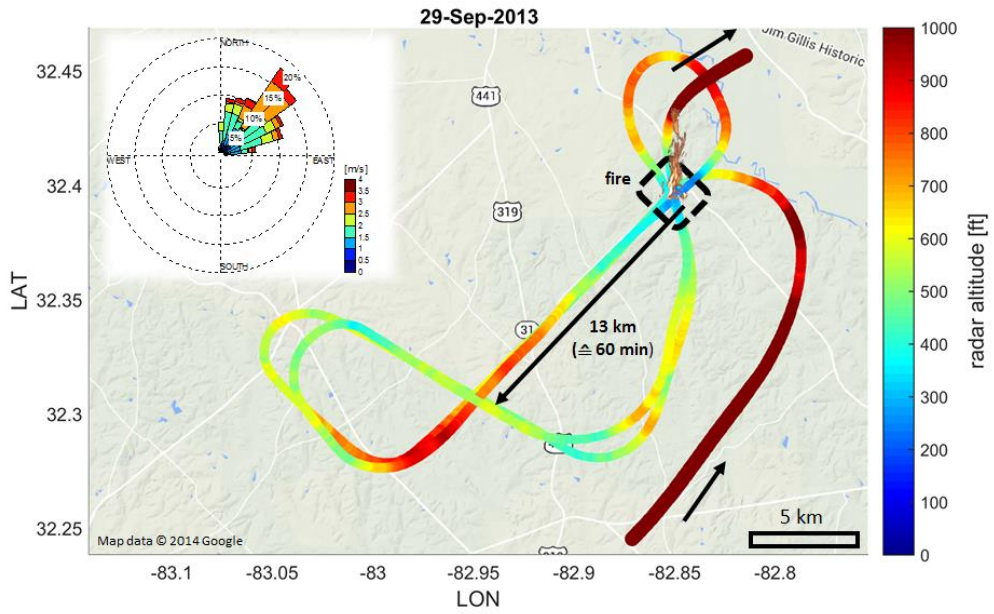

Figure 2. Flight pattern of the NASA P-3B to obtain four point source emission profiles, two longitudinal plume transects (source to 1 hour downwind) and two transverse downwind plume transects (1 hour downwind from source). The inset shows wind rose data obtained during the two longitudinal plume transects when wind measurements are most accurate.

The fire was sighted and approached from the SW. Following a 180° turn, the aircraft overflew the fire for the first time at 125 m altitude (Figure 1a) at 17:33:35 UTC (source emission profile 1). The plume was then followed downwind in southwesterly direction for approximately 2 minutes, slowly climbing in altitude to reach a radar altitude of 190 m at a 13.6 km downwind location (longitudinal plume transect 1). The underlying terrain was forested and agricultural land. At an average wind speed of 3.5 ms^{-1}, the plume travel time for a 13.6 km distance is approximately one hour. Following a horizontal loop maneuver, the ~ 8 km broad plume was sampled transversely at 160 m radar altitude at the 13.6 km downwind location (transverse downwind plume transect 1). Subsequently, the P-3B returned to the fire intercepting the freshly emitted plume at 17:42:57 UTC (Figure 1b) and at 17:45:38 UTC, at 110 m and 80 m altitude respectively (source emission profiles 2 and 3). The downwind pattern was repeated with longitudinal plume transect 2 reaching 220 m altitude at the 13.6 km downwind location. The second transverse downwind plume transect was at 160 m altitude at the 13.6 km downwind location. The fourth and final fire overflight was at 75 m

altitude at 17:54:25 UTC (source emission profile 4). By implementing this sampling strategy, we obtained i) four source emission profiles within 21 minutes, ii) two longitudinal plume transects (source to 1 hour downwind) and iii) four plume characterizations at 1 hour downwind distance from source (two longitudinal "spot" samples and two "integrated" cross-plume samples). The results (see Section 3) indicate near-stable source conditions during the sampling period. This implies that the observed downwind differences were mostly due to dilution and photochemistry.

2.2 Analytical instrumentation

The NASA P-3B was returning from a DISCOVER-AQ deployment (http://discover-aq.larc.nasa.gov/) in Houston, which had it equipped with a payload for *in-situ* atmospheric chemistry measurements. The data used in this study were obtained using the analytical instruments listed in Table 1.

Table 1. Excerpt of the P-3B analytical chemistry payload.

Instrument acronym	Measurement principle	Analyte*	Accuracy	Reference
PTR-ToF-MS	chemical ionization	NMOGs, HONO, NH_3	5-40%	Müller et al., 2014
$NOxyO_3$	chemiluminescence	NO	10 pptV + 10%	Ridley and Grahek, 1990
		NO_2	20 pptV + 10%	
		NO_y	50 pptV + 20%	
		O_3	0.1 ppbV + 5%	
AVOCET	non-dispersive IR spectroscopy	CO_2	0.25 ppmV	Vay et al., 2011
DACOM	differential absorption spectroscopy	CO	< 1 ppbV	Sachse et al., 1987
		CH_4		
UHSAS	laser-based optical-scattering	sub-µm particle size distribution	20%	Cai et al., 2008

* Measurement frequency was 1 Hz for instruments except PTR-ToF-MS (10 Hz).

This work focuses on NMOGs as measured by the PTR-ToF-MS instrument described in detail by Müller et al. (2014). The data presented herein were acquired at a frequency of 10 Hz, which makes the PTR-ToF-MS instrument ideally suited for airborne NMOG measurements at high spatio-temporal resolution. However, only the elemental composition of organic analytes can be determined and not their structure. In other words, the PTR-ToF-MS instrument does not resolve isomeric NMOGs (e.g. acetic acid and glycolaldehyde). The PTR-TOF Data Analyzer Toolbox (https://sites.google.com/site/ptrtof/) was used for data analysis (Müller et al., 2013). Accurate *m/z* information, element restriction to C, H, N and O atoms

and isotopic pattern analyses were used to determine the elemental composition ($C_wH_xN_yO_z$) of detected analyte ions. It has been shown in previous work that accurate *m/z* information can be obtained even at a moderate mass resolution m/Δm in the range of 1000 to 1500 (Müller et al., 2011, 2014). The assignment of observed *m/z* signals to specific chemical compounds was based on the literature (see paragraph 3.1.2).

Methanol, acetonitrile, acetaldehyde, acetone, isoprene, methyl ethyl ketone, benzene, toluene, m-xylene, 1,3,5-trimethylbenzene and monoterpenes (α-pinene) were calibrated externally using a dynamically diluted certified standard. The measurement accuracy is ± 5% for pure hydrocarbons and ± 10% for oxygenates. Formic acid and acetic acid were calibrated (± 10%) in a post-campaign study using a liquid standard nebulization device (LCU, Ionicon Analytik, Austria). The protonated formaldehyde ion signal was cross-calibrated to formaldehyde data collected by a Difference Frequency Absorption Spectroscopy (DFGAS, Weibring et al. (2007)) instrument during the same flight and at the same humidity conditions. Although less accurate (±10%), PTR-ToF-MS formaldehyde data were used instead of DFGAS observations because of a higher data density in the plume. Instrumental response factors to furan, methylglyoxal and 2-furfural were calculated from ion-molecule collision theory (Cappellin et al., 2012). The estimated measurement accuracy for these species is ±25%. Peroxyacetyl nitrate (PAN) was quantified (± 40%) using a calibration factor obtained in a previous study (unpublished data). All other organic signals were corrected for instrumental mass discrimination effects and converted to volume mixing ratios by using the acetone sensitivity as a proxy. Mixing ratios in acetone-equivalents are estimated to be accurate to within ±40%. This is also the maximum error we must assume for the total NMOG mass calculated by summing all individual signals calibrated as specified above.

The PTR-ToF-MS instrument also detects a few inorganic gases, nitrous acid (HONO) and ammonia (NH_3) being two prominent examples. Given the importance of HONO for fire plume photochemistry, we made an attempt to quantify HONO emissions. HONO dehydrates upon protonation forming NO^+ ions, which are observed at *m/z* 29.997. The excess NO^+ signal in the plume was assigned to HONO. The contribution from organic nitrites was assumed to be minor. A positive measurement artifact from NO_2-to-HONO conversion (1% of NO_2) on instrumental surfaces was subtracted. The instrumental response to HONO and HONO inlet artifacts have been characterized in previous studies (Metzger et al., 2008;

Wisthaler et al., 2003). Given that different inlet and drift tube configurations were used in those studies, the 1% NO_2-to-HONO conversion efficiency is to be considered an upper limit estimate. Still, the NO_2-artifact only accounts for 10.4% of the NO^+ signal measured at the source. The estimated accuracy of the reported HONO data is ±30%. NH_3 measurements suffered from a high intrinsic background signal generated in the ion source of the instrument. This deteriorated the detection limit to 12 ppbV for 1-Hz measurements.

2.3 Data processing

Volume mixing ratios (VMRs) were obtained as described in section 2.2. When referring to the VMR of a species X, the italic style, *X*, is used throughout this work.

Given that the P-3B spent about two seconds in the plume during fire overflights and that CO was only measured at 1 Hz, it was not possible to perform linear regression analyses, *X* vs. *CO*, on data from individual plume intercepts. For each plume intercept, we calculated the excess mixing ratio of X in the fire plume, ΔX, as the average mixing ratio of X inside the plume, $\overline{X}_{plume}$, minus the average mixing ratio of X outside the plume, $\overline{X}_{background}$:

$$\Delta X = \overline{X}_{plume} - \overline{X}_{background}$$

$\overline{X}_{background}$ was calculated from the data obtained immediately before plume interception. Background mixing ratios of all species discussed herein were stable in the investigated domain. This analysis was performed for each of the fire overflights resulting in four data points, ΔX vs. ΔCO, for source emission characterization~~This analysis resulted in four data points, ΔX vs. ΔCO, for characterizing source emission profiles~~. A linear least-square regression analysis was then applied to these four data points, with the slope of the regression line describing the molar emission ratio (ER) of the species X relative to CO, $ER_{X/CO}$, in ppbV $ppmV^{-1}$. The precision of the CO data is better than ±1 ppbV which justifies the use of a univariate regression method. The standard error of the slope reflects both the natural variability in the plume and the measurement imprecision. A delayed instrument response was observed for formic acid and acetic acid. In-plume concentrations of these acids were derived as discussed in the Supplement.

The dilution-corrected molar excess mixing ratio of a species X, $\Delta_{dil}X$ (in ppbV), at a downwind location was calculated from the excess mixing ratio of CO observed at the fire source, ΔCO_{source}, and the locally observed ΔX and ΔCO using the following equation:

$$\Delta_{dil}X = \Delta X \frac{\Delta CO_{source}}{\Delta CO}$$

By introducing this parameter, we are able to study loss or formation processes in the plume without confounding contributions from dilution. On a one-hour timescale, no photochemical loss of CO occurs and the contribution from photochemically formed CO to the large CO levels already present in the plume is negligible. Reported $\Delta_{dil}X$ are average values from two longitudinal plume transects for which data were binned at 1 km spatial resolution.

The emission factor of a species X, EF_X, in g/kg was calculated according to Yokelson et al. (1999):

$$EF_X = F_c \text{ x } 1000 \text{ x} \frac{MM_X}{MM_C} \text{ x } \frac{C_X}{C_T}$$

with F_C being the mass fraction of carbon of the fuel, MM_X and MM_C the molecular masses of the species X and of carbon, and C_X/C_T the fraction of moles emitted as species X relative to the total number of moles carbon emitted. F_C was not measured during this study but 0.50 is a typical value for biomass (Burling et al., 2010). The accuracy of C_T is limited by unmeasured carbon. This fraction is assumed to be less than 2%. EFs were calculated as averages from the four fire overflights.

The oxygen-to-carbon (O:C) ratio of all detected NMOGs was calculated as follows:

$$\frac{O}{C} = \frac{\sum_i n_{O,i} X_i}{\sum_i n_{C,i} X_i}$$

with $n_{O,i}$ and $n_{C,i}$ being the number of oxygen atoms and carbon atoms in the species X_i, respectively.

The modified combustion efficiency (MCE) was calculated as follows (Ferek et al., 1998):

$$MCE = \frac{\Delta CO_2}{\Delta CO + \Delta CO_2}$$

Aerosol mass was calculated from the 60-1000 nm integrated optical aerosol volume as measured by the UHSAS instrument assuming an average biomass burning secondary organic aerosol density of 1.3 g cm^{-3} (Aiken et al., 2008).

2.4 Chemical box model calculations

We used the University of Washington Chemical Box Model (UWCM) (Wolfe and Thornton, 2011) run on Master Chemical Mechanism (MCM) v3.3 chemistry (Jenkin et al., 1997, 2003, 2015; Saunders et al., 2003) to simulate the downwind processing of trace gases in the biomass burning plume. The model was initialized using measured source concentrations of NO, NO_2, HONO, O_3, CO, CH_4 and of the 16 most abundant NMOGs detected by PTR-ToF-MS ($ER_{X/CO}$ > 1.0 ppbV $ppmV^{-1}$; compounds identified in previous studies as detailed in paragraph 3.1.2). The model was run using the measured meteorological parameters (pressure, temperature, relative humidity, solar zenith angle) and the observed NO_2 photolysis rate. The model calculates dilution from the simple equation

$$\frac{dX}{dt} = -k_{dil}\left(X(t) - \bar{X}_{background}\right)$$

where k_{dil} represents the dilution rate coefficient obtained from the decrease of ΔCO versus plume travel time. k_{dil} was calculated in 285 s time bins (equivalent to 1 km distance bins). More information on the UWCM and the underlying theory can be found in Dillon et al. (2002), Wolfe and Thornton (2011) and Wolfe et al. (2012). ~~The dilution rate was obtained from the measured molar excess mixing ratios of CO.~~ MCM v3.3 chemistry does not include the degradation of furan and 2-furfural, two highly reactive compounds with significant primary emissions from fires. We included these species in our chemical mechanism using the photolysis rates reported by Colmenar et al. (2015) and the OH reaction rates reported by Bierbach et al. (1992). We assumed that butenedial is the only primary reaction product of the reaction of furan with OH radicals (Aschmann et al., 2014). The atmospheric oxidation products of 2-furfural are unknown.

3 Results and discussion

3.1 Emissions

3.1.1 Inorganic gases

Table 2 summarizes $ER_{X/CO}$ and EF_X values of major inorganic gases as obtained from four source emission profiles. An MCE of 0.90 ± 0.02 was derived from the measured CO and CO_2 data indicating stable burning conditions and roughly equal amounts of biomass consumption by flaming and smoldering combustion.

Table 2. Molar emission ratios (ER) relative to CO and emission factors (EF) of the major inorganic gases as obtained from four fire overflights.

compound	$ER_{X/CO}$	EF_X (g/kg)
CO_2	--	1623 ± 68
CO	--	94.6 ± 31.3
NO	10.4 ± 5.2	0.63 ± 0.51
NO_2	9.4 ± 2.0	1.24 ± 0.06
HONO	2.0 ± 0.7	0.15 ± 0.05
NH_3	< 5.2	< 0.73

ERs and EFs of NO and NO_2 are within typical ranges reported in the literature (Akagi et al., 2011). The observed $ER_{HONO/CO}$ of 2.0 ± 0.7 ppbV $ppmV^{-1}$ is also in good agreement with previously reported values (e.g. Veres et al., 2010) increasing our confidence in the tentative identification and quantification of HONO emissions by PTR-ToF-MS. Excess mixing ratios of NH_3 in the plume were below the detection limit so that only an upper limit for $ER_{NH3/CO}$ and EF_{NH3} is reported.

3.1.2 Organic gases

Methane (CH_4) was the main organic gas emitted from the fire. $ER_{CH4/CO}$ and EF_{CH4} are 108.4 ± 13.4 ppbV $ppmV^{-1}$ and 6.25 ± 2.86 g/kg, respectively. This work, however, focuses on NMOG emissions. Figure 3a shows the 10 Hz time series of acetonitrile (CH_3CN), furan (C_4H_4O), sum of monoterpene isomers ($C_{10}H_{16}$) and isoprene (C_5H_8) as measured during the overflight at 17:54:25 UTC (source emission profile 4). Figure 3b shows the time series of benzene (C_6H_6), toluene (C_7H_8), C_8-alkylbenzene isomers (C_8H_{10}) and C_9-alkylbenzene

isomers (C_9H_{12}) for the same time period. The data demonstrate that the airborne PTR-ToF-MS instrument generates high-precision NMOG data even for very localized emission sources. The two small plumes discernible in Figures 1a and 1b are well resolved in the PTR-ToF-MS data shown in Figure 3. All signals instantly drop to background levels outside the plume confirming the excellent time response of the airborne PTR-ToF-MS instrument for analytes that do not adhere to instrumental surfaces.

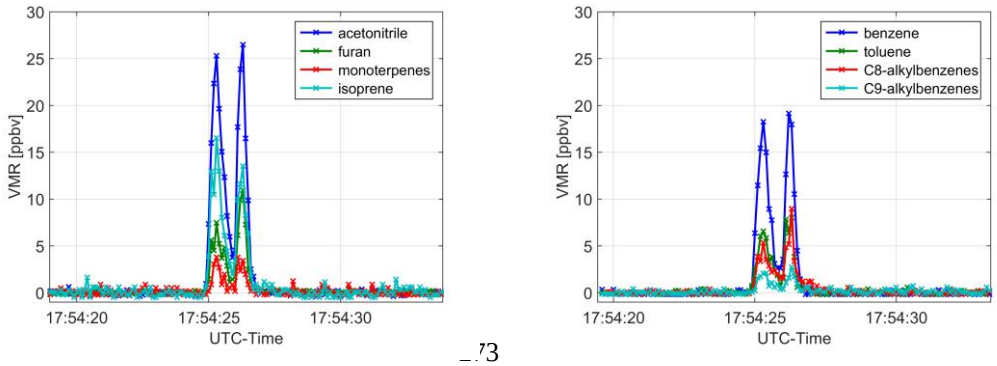

Figure 3. 10 Hz time-series of (a) acetonitrile, furan, the sum of monoterpene isomers and isoprene and (b) benzene, toluene, C_8-alkylbenzene isomers and C_9-alkylbenzene isomers as measured during the fourth fire overflight at 17:54:25 UTC.

It is currently not possible to fully exploit these highly time resolved NMOG data for determining $ER_{X/CO}$ because CO is only measured at 1-second time resolution. $ER_{X/CO}$ values were thus obtained from average values for each source emission profile as described in section 2.3.

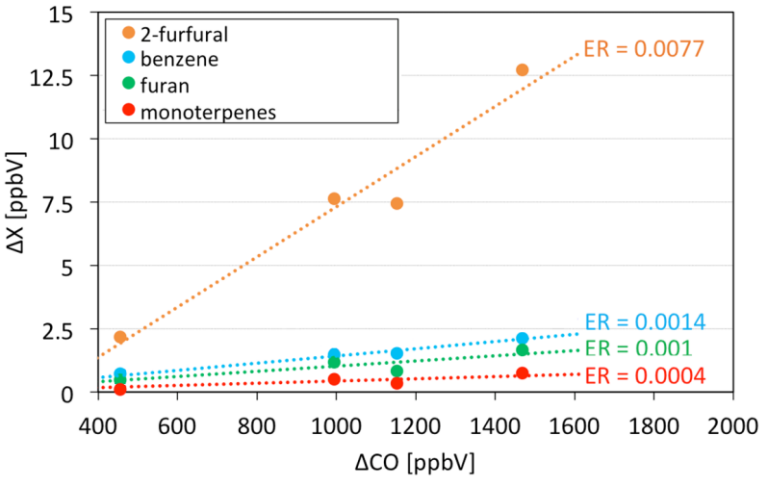

Figure 4. Average excess VMRs of 2-furfural, benzene, furan, and monoterpenes versus average excess VMRs of CO. Each data point represents data from one fire overflight (source emission profile). The slopes of the least-square regressions (dotted lines) correspond to the initial molar emission ratios ($ER_{X/CO}$, in ppbV/ppbV).

Figure 4 shows ΔX vs. ΔCO as obtained for 2-furfural, benzene, furan, and monoterpenes during each of the four fire overflights. The compounds were selected as representatives of different chemical classes (including furans, aromatics, aldehydes, terpenes) that can have different production mechanisms in the fire, e.g. furan being formed by pyrolysis and monoterpenes just being evaporated (Yokelson et al., 1996). A strong linear relationship was found not only for the species shown here but for all detected NMOGs indicating that source emissions were near-stable during the 21 minute sampling period. This important finding will later allow us to draw conclusions from analyte ratios measured downwind.

In total, 57 *m/z* signals (NO^+, NO_2^+ and 55 C-containing ions) in the PTR-ToF-MS spectrum showed an enhancement in the source emission profiles. Table 3 lists $ER_{X/CO}$ and EF_X of the 18 ion signals that contain carbon atoms and that were observed with an $ER_{X/CO}$ > 1 ppbV $ppmV^{-1}$. These signals contribute 93% of the total NMOG emissions as detected by PTR-ToF-MS. Emissions are dominated by formaldehyde, methanol, acetaldehyde and 2-furfural (EF > 1 g kg^{-1}). The complete list of all detected ion signals is given in Table S1 in the Supplement.

Table 3. Measured accurate *m/z*, elemental composition $C_wH_xN_yO_z^+$ of the detected ion, neutral precursor assignment based on literature information (significant interferants in

parentheses, tentative assignments in italic), emission factor (EF) and standard deviation (SD), emission ratio (ER) and standard deviation for all detected NMOGs with $ER_{X/CO}$ > 1 ppbV $ppmV^{-1}$.

m/z	elemental composition	neutral precursor	EF	SD	ER	SD
			[g/kg]		[ppbV/ppmV]	
31.018	CH_3O^+	formaldehyde	2.31	0.57	22.7	1.3
33.034	CH_5O^+	methanol	2.25	1.06	19.6	2.0
42.034	$C_2H_4N^+$	acetonitrile	0.19	0.06	1.5	0.2
43.055	$C_3H_7^+$	propene (other unknown precursors)	0.64	0.25	4.5	0.2
45.034	$C_2H_5O^+$	acetaldehyde	1.52	0.50	10.4	0.3
47.020	$CH_3O_2^+$	formic acid	≤0.13	0.38	≤1.4	0.6
59.050	$C_3H_7O^+$	acetone (propanal)	0.83	0.31	4.1	0.1
61.029	$C_2H_5O_2^+$	acetic acid (glycolaldehyde)	0.47	0.18	2.7	0.3
69.034	$C_4H_5O^+$	furan	0.25	0.12	1.0	0.1
69.070	$C_5H_9^+$	isoprene (pentadienes, cyclopentene)	0.23	0.14	1.1	0.1
71.050	$C_4H_7O^+$	MVK (crotonaldehyde, MACR)	0.33	0.12	1.4	0.0
73.024	$C_3H_5O_2^+$	methylglyoxal	0.27	0.07	1.2	0.1
75.044	$C_3H_7O_2^+$	hydroxy acetone (methyl acetate, propionic acid)	0.28	0.15	1.1	0.1
79.055	$C_6H_7^+$	benzene	0.40	0.15	1.4	0.0
85.027	$C_4H_5O_2^+$	*dioxin, furanone*	0.39	0.12	1.5	0.1
87.043	$C_4H_7O_2^+$	2,3-butandione	0.44	0.18	1.6	0.1
97.029	$C_5H_5O_2^+$	2-furfural	2.31	1.07	7.7	0.6
111.041	$C_6H_7O_2^+$	*benzenediols, methylfurfural*	0.39	0.21	1.2	0.1

It is beyond the scope and possibilities of this work to make an independent assignment of *m/z* signals to specific neutral precursors. The P-3B payload did not include any NMOG analyzer with higher analytical selectivity than the PTR-ToF-MS instrument. Our assignment of *m/z* signals to specific chemicals in Tables 3 and S2 thus exclusively relies on two recent studies and the references used therein. Yokelson et al. (2013) used results from multiple analytical techniques for assigning *m/z* peaks. Stockwell et al. (2015) used a high mass resolution PTR-ToF-MS instrument for elemental composition determination and open-path FTIR data together with literature reports for mass spectral interpretation. In the case of multiple neutral precursors for a specific *m/z* signal, we considered only species with a relative contribution > 10 % to the total signal. Two ion signals (*m/z* 85.027 and *m/z* 111.041) were not reported previously. The assignment made is tentative and the compounds (in italic) were not included in the modeling study. The reader is cautioned that this is still an evolving field of research and some signals may be misassigned or suffer from yet unknown interferences.

Total observed carbon emitted as NMOGs (55 ion signals) was 10,472 ppbC. The O/C ratio at the fire source was 0.41. Figure 5 shows the relative contribution of C_1 to C_{10} compounds to total NMOG emissions on a carbon atom basis.

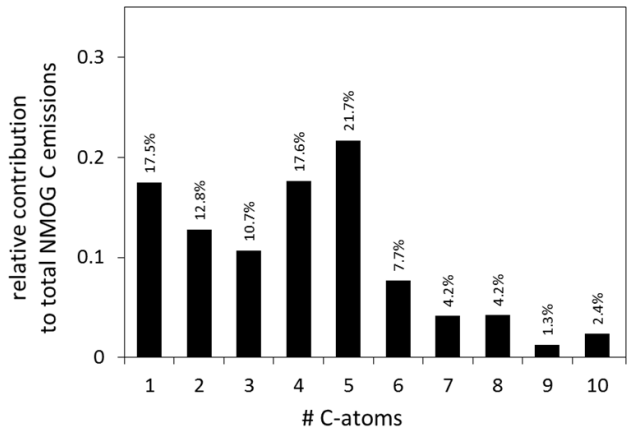

Figure 5. Relative contributions of C_1-C_{10} compounds to total NMOG carbon emissions. C_1 to C_5 compounds each have relative contributions > 10%, and in sum contribute ~ 80% of the total NMOG carbon emissions.

The dominant contribution to NMOG carbon emissions came from the C_5-compound 2-furfural. Significant carbon emissions ($ER_{X/CO}$ > 50 pptV $ppmV^{-1}$) were detected only up to C_{10} (monoterpenes).

3.2 Plume evolution

The NASA P-3B sampled the downwind plume for approximately 2 minutes of flight time. At an average wind speed of 3.5 m s^{-1}, this corresponds to approximately one hour of atmospheric plume processing. Volume mixing ratios of inert tracers (CO_2, CO, acetonitrile and benzene) consistently decreased by a factor of ~ 13.5 during the two longitudinal plume transects. We used this decrease to derive dilution-corrected molar excess mixing ratio of reactive trace gas species X, $\Delta_{dil}X$ (see paragraph 2.3). $\Delta_{dil}X$ were used to investigate downwind plume chemistry by observations and by a 0-D photochemical box model simulation initialized with measured emission data.

3.2.1 Ozone formation and sequestration of nitrogen oxides

Figure 6 shows dilution-corrected molar excess mixing ratios of O_3, NO, NO_2 and NO_z (=NO_y-NO-NO_2) during one hour of atmospheric plume processing. Point symbols refer to the measured data; solid lines represent the output of the UWCM based on MCM v3.3 chemistry.

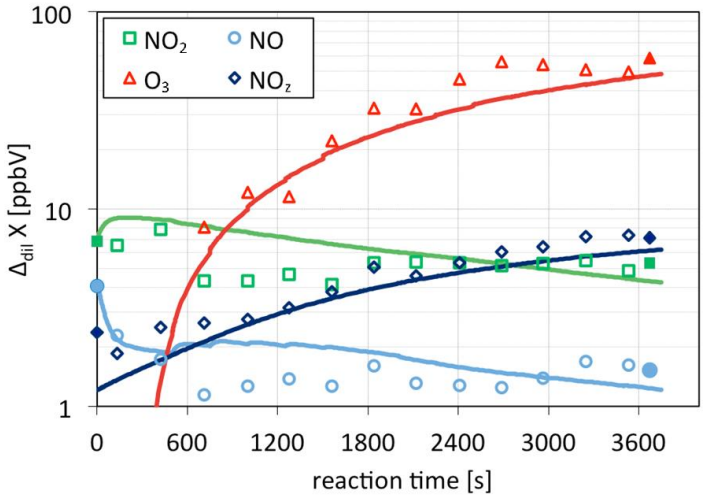

Figure 6. Dilution-corrected molar excess mixing ratios of O_3, NO, NO_2 and NO_z (= NO_y-NO-NO_2) during one hour of plume evolution (in one kilometer bins). Point symbols refer to the measured data; solid lines represent the output of the UWCM based on MCM v3.3 chemistry.

Ozone is efficiently formed in the plume in the presence of NO_x and NMOGs. Close to the source (t < 600 s), ambient O_3 reacts with abundantly emitted NO resulting in negative O_3 excess mixing ratios (not displayed on the logarithmic ordinate of Figure 6). After ~ 10 minutes of plume processing net ozone formation starts, resulting in a dilution-corrected increase of O_3 on the order of 50-60 ppbV during the first hour the plume resides in the atmosphere. The UWCM (MCM v3.3 chemistry; initialized with measured emissions of NO, NO_2, HONO, O_3, CO, CH_4 and 16 NMOGs) simulates the evolution of O_3, NO and NO_2 well. An even better agreement in the ozone evolution is obtained if the model is constrained to measured formaldehyde values which slightly exceed the modeled values at t > 1500 s (see see paragraph 3.2.2). O_3 formation is fueled by HO_2/CH_3O_2+NO reactions. The model indicates that HO_2 radicals are primarily generated in the CO+OH, 2-furfural+OH and formaldehyde+OH reactions. CH_3O_2 radicals are primarily formed in the $CH_3C(O)O_2$+NO

and CH_4+OH reactions; the main precursors of $CH_3C(O)O_2$ radicals are acetaldehyde, 2,3-butanedione and methylglyoxal.

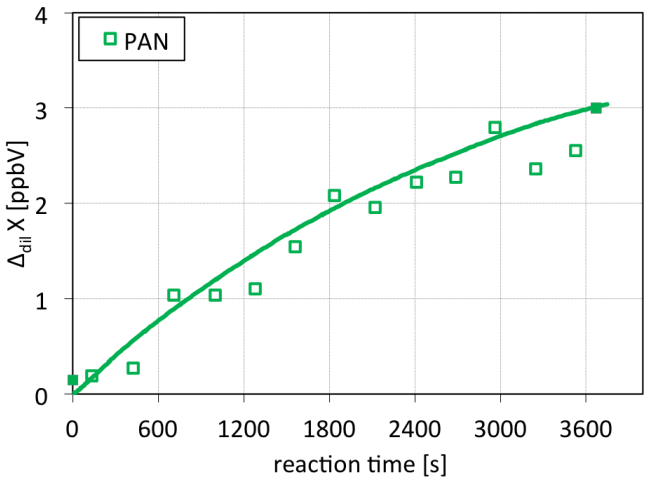

Figure 7. Dilution-corrected molar excess mixing ratios of PAN during one hour of plume evolution (in one kilometer bins). Point symbols refer to the measured data; the solid line represents the output of the UWCM based on MCM v3.3 chemistry.

The model also accurately captures the net formation of NO_z (= NO_y-NO-NO_2). Modelled NO_z sums all species in the MCM v3.3 degradation scheme that include nitro or nitroso groups. The main contributors to NO_z being formed are peroxyacetyl nitrate (PAN) and nitric acid (HNO_3). The model simulates $\Delta_{dil}PAN$ = 3 ppbV and $\Delta_{dil}HNO_3$ = 2.4 ppbV after one hour of plume evolution which accounts for ~ 90% of all NO_z formed. Under the operating conditions used in this study, PAN is predominantly detected at *m/z* 45.992 (NO_2^+) by the PTR-ToF-MS instrument (Hansel and Wisthaler, 2000). Using a PAN calibration factor obtained in a previous study, we obtain an excellent agreement between measured and modeled PAN concentrations (Figure 7).

3.2.2 Evolution of NMOGs

Fire emissions include many NMOGs that quickly react with OH radicals. OH radicals are abundantly formed in biomass burning plumes causing highly reactive NMOGs to disappear even on the one-hour time scale investigated in this study (Akagi et al., 2012, 2013; Hobbs et al., 2003). Figure 8 shows dilution-corrected mixing ratios of furan and 2-furfural during one

hour of plume evolution. Point symbols refer to the dilution-corrected experimental data; solid lines represent the output of the UWCM. Measured and modeled data are in excellent agreement confirming that we observed the OH-initiated degradation of furan and 2-furfural. The influence of interfering isomers (or fragment ions), if any, is small. The box model output indicates near-stable OH radical concentrations of 7.45 ± 1.07 x10^6 cm^{-3} along the 13 km downwind transect. Other studies (eg. Yokelson et al., 2009) have reported similarly high average OH levels in biomass burning plumes.

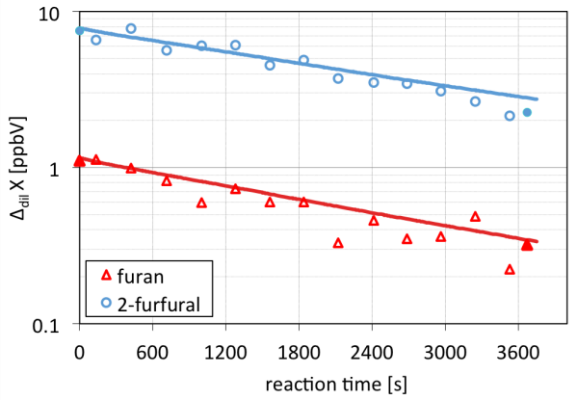

Figure 8. Dilution-corrected molar excess mixing ratios of furan and 2-furfural during one hour of plume evolution. Point symbols refer to the measured data (one kilometer bins); solid lines represent the output of the UWCM fed with MCM v3.3 chemistry.

Figure 9 shows dilution-corrected mixing ratios of four important oxygenated NMOGs, formaldehyde, acetaldehyde, methanol and acetone/propanal. Point symbols again refer to the dilution-corrected experimental data; solid lines represent the output of the UWCM. Formaldehyde and acetone/propanal show a distinct increase after half an hour of plume processing, which is not captured by the model simulation based on MCM v3.3 degradation chemistry of the 16 most abundant NMOGs (as detected by PTR-ToF-MS). Interestingly, the experimental data indicate a significant loss of methanol during the initial 15 minutes of plume processing. This sink is also not included in MCM v3.3 chemistry and heterogeneous loss processes should be investigated. The observed initial drop could, however, also be caused by an unknown highly reactive compound that interferes with the detection of methanol. In addition to the carbonyls discussed above, acetic acid/glycolaldehyde and the $C_4H_3O_3^+$ signal, which is tentatively assigned to maleic acid/maleic anhydride, exhibited

dilution-corrected increases of ~ 1.5 ppbV and ~ 1 ppbV, respectively. The model was unable to capture the observed increase. This does not come as a surprise since these species are typical higher-order degradation products that are not included in MCM v3.3 degradation schemes.

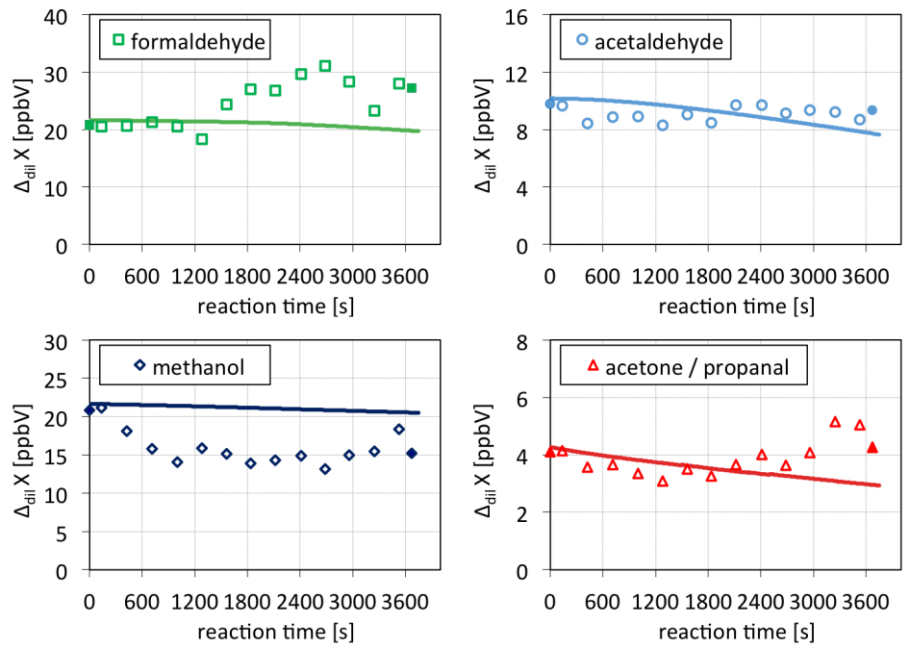

Figure 9. Dilution-corrected molar excess mixing ratios of formaldehyde (a), acetaldehyde (b), methanol (c), and acetone/propanal (d) during one hour of plume evolution. Point symbols refer to the measured data (one kilometer bins); solid lines represent the output of the UWCM fed with MCM v3.3 chemistry.

Figure 10 compares the relative contributions of C_1 to C_{12} compounds to total NMOG carbon measured at the fire source and at the 1-hour downwind location. C_1, C_2 and C_4 compounds exhibited the largest relative increase. The observed O/C ratio at the 1-hour downwind location source was 0.56, compared to 0.41 observed at the source. This is consistent with the conceptual picture of a photochemical breakdown of NMOGs into smaller, more oxidized species.

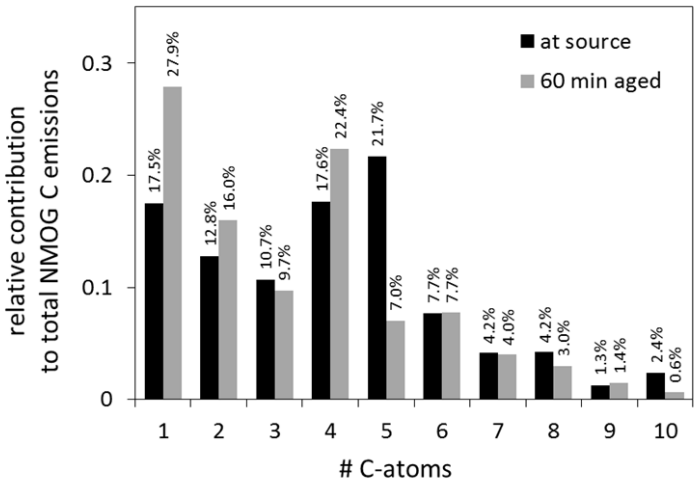

Figure 10. Relative contributions of C_1 to C_{12} compounds to total NMOG carbon measured at the fire source and at the 1-hour downwind location.

3.2.3 Gas-to-particle conversion

A dilution-corrected mass balance analysis reveals that 40.8 µg cm^{-3} of the mass initially emitted as NMOGs was lost during one hour of atmospheric processing. This equals 24% of the carbon initially emitted as NMOGs. At the same time, the dilution-corrected total particle mass concentration as derived from UHSAS measurements increased by ~78 µg m^{-3}. These mass concentration calculations are only approximate (for details see paragraph 2.2), but this analysis suggests that about 50% of the aerosol mass formed in the downwind plume is organic in nature. This agrees with findings from previous studies that observed significant organic and inorganic aerosol formation in aging biomass burning plumes (Cubison et al., 2011; Yokelson et al., 2009). Given that photo-oxidation of 2-furfural has the highest mass turnover, secondary organic aerosol formation from the 2-furfural + OH reaction should be investigated in laboratory experiments.

4 Summary and Conclusion

A plume emanating from a small forest understory fire was investigated in an airborne study. High spatio-temporal resolution data were obtained for inorganic and organic trace gases, the latter being sampled for the first time at 10 Hz using a PTR-ToF-MS instrument. We generated quantitative emission data for CO_2, CO, NO, NO_2, HONO, NH_3 and 16 NMOGs

with $ER_{X/CO}$ > 1.0 ppbV $ppmV^{-1}$. NMOG emissions were dominated by formaldehyde, acetaldehyde, 2-furfural and methanol. No NMOGs with more than 10 carbon atoms were observed at mixing ratios larger than 50 pptV per ppmV CO emitted. Downwind plume chemistry was investigated both by observations and by a model simulation using near-explicit MCM v3.3 chemistry. The observed dilution-corrected O_3 increase on the order of 50-60 ppbV was well captured by the model, which indicated carbonyls (formaldehyde, acetaldehyde, 2,3-butanedione, methylglyoxal, 2-furfural) in addition to CO and CH_4 as the main drivers of peroxy radical chemistry. The model also accurately reproduced the sequestration of NO_x into PAN and the degradation of furan and 2-furfural at average OH plume concentrations of 7.45±1.07 $x10^6$ cm^{-3}. Formaldehyde, acetone/propanal, acetic acid/glycolaldehyde and maleic acid/maleic anhydride (tentative identification) were found to increase during one hour of atmospheric plume processing, with the model being unable to capture the increase. A dilution-corrected mass balance analysis suggests that about 50% of the aerosol mass formed in the downwind plume is secondary organic in nature.

We conclude that the PTR-ToF-MS instrument is a powerful analytical tool for airborne plume studies. The generated data are highly valuable in characterizing point source emissions and near-field chemical transformations. Key chemical processes (ozone and radical formation, NOx sequestration) in an aging biomass burning plume were accurately simulated using a 0-D photochemical box model run with up-to-date and near-explicit MCM v3.3 chemistry.

Acknowledgements

This work was primarily funded through the Austrian Space Applications Programme (ASAP 8 and 9, grants #833451 and #840086). ASAP is sponsored by the Austrian Ministry for Transport, Innovation and Technology (BMVIT) and administered by the Aeronautics and Space Agency (ALR) of the Austrian Research Promotion Agency (FFG). P. Eichler was funded through the PIMMS ITN supported by the European Commission's 7th Framework Programme under grant agreement number 287382. T. Mikoviny was supported by an appointment to the NASA Postdoctoral Program at the Langley Research Center, administered by Oak Ridge Associated Universities through a contract with NASA. A. Wisthaler received support from the Visiting Scientist Program of the National Institute of Aerospace (NIA). R. Yokelson acknowledges support by NASA Earth Science Division

Awards NNX12AC20G and NNX14AP45G. DISCOVER-AQ was part of the NASA Earth Venture-1 (EV-1) program. John Barrick is acknowledged for providing wind data and camera images. The authors would like to thank the pilots and crew of NASA's P-3B and J. Raymond Joyce, Laurens County Extension Agent, for local inspection of the fire. DISCOVER-AQ data can be obtained from the NASA Langley Research Center Atmospheric Science Data Center (doi:10.5067/Aircraft/DISCOVER-AQ/Aerosol-TraceGas).

References

Aiken, A. C., DeCarlo, P. F., Kroll, J. H., Worsnop, D. R., Huffman, J. A., Docherty, K. S., Ulbrich, I. M., Mohr, C., Kimmel, J. R., Sueper, D., Sun, Y., Zhang, Q., Trimborn, A., Northway, M., Ziemann, P. J., Canagaratna, M. R., Onasch, T. B., Alfarra, M. R., Prevot, A. S. H., Dommen, J., Duplissy, J., Metzger, A., Baltensperger, U. and Jimenez, J. L.: O/C and OM/OC Ratios of Primary, Secondary, and Ambient Organic Aerosols with High-Resolution Time-of-Flight Aerosol Mass Spectrometry, Environ. Sci. Technol., 42(12), 4478–4485, doi:10.1021/es703009q, 2008.

Akagi, S. K., Yokelson, R. J., Wiedinmyer, C., Alvarado, M. J., Reid, J. S., Karl, T., Crounse, J. D. and Wennberg, P. O.: Emission factors for open and domestic biomass burning for use in atmospheric models, Atmospheric Chem. Phys., 11(9), 4039–4072, doi:10.5194/acp-11-4039-2011, 2011.

Akagi, S. K., Craven, J. S., Taylor, J. W., McMeeking, G. R., Yokelson, R. J., Burling, I. R., Urbanski, S. P., Wold, C. E., Seinfeld, J. H., Coe, H., Alvarado, M. J. and Weise, D. R.: Evolution of trace gases and particles emitted by a chaparral fire in California, Atmos Chem Phys, 12(3), 1397–1421, doi:10.5194/acp-12-1397-2012, 2012.

Akagi, S. K., Yokelson, R. J., Burling, I. R., Meinardi, S., Simpson, I., Blake, D. R., McMeeking, G. R., Sullivan, A., Lee, T., Kreidenweis, S., Urbanski, S., Reardon, J., Griffith, D. W. T., Johnson, T. J. and Weise, D. R.: Measurements of reactive trace gases and variable O3 formation rates in some South Carolina biomass burning plumes, Atmos Chem Phys, 13(3), 1141–1165, doi:10.5194/acp-13-1141-2013, 2013.

Aschmann, S. M., Nishino, N., Arey, J. and Atkinson, R.: Products of the OH Radical-Initiated Reactions of Furan, 2- and 3-Methylfuran, and 2,3- and 2,5-Dimethylfuran in the

Presence of NO, J. Phys. Chem. A, 118(2), 457–466, doi:10.1021/jp410345k, 2014.

Bierbach, A., Barnes, I. and Becker, K. H.: Rate coefficients for the gas-phase reactions of hydroxyl radicals with furan, 2-methylfuran, 2-ethylfuran and 2,5-dimethylfuran at 300 ± 2 K, Atmos. Environ., 26, 813–817, doi:10.1016/0960-1686(92)90241-C, 1992.

Burling, I. R., Yokelson, R. J., Griffith, D. W. T., Johnson, T. J., Veres, P., Roberts, J. M., Warneke, C., Urbanski, S. P., Reardon, J., Weise, D. R., Hao, W. M. and de Gouw, J.: Laboratory measurements of trace gas emissions from biomass burning of fuel types from the southeastern and southwestern United States, Atmos Chem Phys, 10(22), 11115–11130, doi:10.5194/acp-10-11115-2010, 2010.

Cai, Y., Montague, D. C., Mooiweer-Bryan, W. and Deshler, T.: Performance characteristics of the ultra high sensitivity aerosol spectrometer for particles between 55 and 800 nm: Laboratory and field studies, J. Aerosol Sci., 39(9), 759–769, doi:10.1016/j.jaerosci.2008.04.007, 2008.

Cappellin, L., Karl, T., Probst, M., Ismailova, O., Winkler, P. M., Soukoulis, C., Aprea, E., Märk, T. D., Gasperi, F. and Biasioli, F.: On Quantitative Determination of Volatile Organic Compound Concentrations Using Proton Transfer Reaction Time-of-Flight Mass Spectrometry, Environ. Sci. Technol., 46(4), 2283–2290, doi:10.1021/es203985t, 2012.

Colmenar, I., González, S., Jiménez, E., Martín, P., Salgado, S., Cabañas, B. and Albaladejo, J.: UV absorption cross sections between 290 and 380 nm of a series of furanaldehydes: Estimation of their photolysis lifetimes, Atmos. Environ., 103, 1–6, doi:10.1016/j.atmosenv.2014.12.022, 2015.

Cubison, M. J., Ortega, A. M., Hayes, P. L., Farmer, D. K., Day, D., Lechner, M. J., Brune, W. H., Apel, E., Diskin, G. S., Fisher, J. A., Fuelberg, H. E., Hecobian, A., Knapp, D. J., Mikoviny, T., Riemer, D., Sachse, G. W., Sessions, W., Weber, R. J., Weinheimer, A. J., Wisthaler, A. and Jimenez, J. L.: Effects of aging on organic aerosol from open biomass burning smoke in aircraft and laboratory studies, Atmos Chem Phys, 11(23), 12049–12064, doi:10.5194/acp-11-12049-2011, 2011.

Dillon, M. B., Lamanna, M. S., Schade, G. W., Goldstein, A., and Cohen, R. C.: Chemical evolution of the Sacramento urban plume: Transport and oxidation, J. Geophys. Res., 107, 4045, 10.1029/2001JD000969, 2002.

Formatted: Widow/Orphan control, Adjust space between Latin and Asian text, Adjust space between Asian text and numbers

527 Ferek, R. J., Reid, J. S., Hobbs, P. V., Blake, D. R. and Liousse, C.: Emission factors of
528 hydrocarbons, halocarbons, trace gases and particles from biomass burning in Brazil, J.
529 Geophys. Res. Atmospheres, 103(D24), 32107–32118, doi:10.1029/98JD00692, 1998.

530 Hansel, A. and Wisthaler, A.: A method for real-time detection of PAN, PPN and MPAN in
531 ambient air, Geophys. Res. Lett., 27(6), 895–898, doi:10.1029/1999GL010989, 2000.

532 Hobbs, P. V., Sinha, P., Yokelson, R. J., Christian, T. J., Blake, D. R., Gao, S., Kirchstetter, T.
533 W., Novakov, T. and Pilewskie, P.: Evolution of gases and particles from a savanna fire in
534 South Africa, J. Geophys. Res. Atmospheres, 108(D13), 8485, doi:10.1029/2002JD002352,
535 2003.

536 Huffman, J. A., Docherty, K. S., Aiken, A. C., Cubison, M. J., Ulbrich, I. M., DeCarlo, P. F.,
537 Sueper, D., Jayne, J. T., Worsnop, D. R., Ziemann, P. J. and Jimenez, J. L.: Chemically-
538 resolved aerosol volatility measurements from two megacity field studies, Atmos Chem Phys,
539 9(18), 7161–7182, doi:10.5194/acp-9-7161-2009, 2009.

540 Jenkin, M. E., Saunders, S. M. and Pilling, M. J.: The tropospheric degradation of volatile
541 organic compounds: A protocol for mechanism development, Atmos. Environ., 31(1), 81–
542 104, doi:10.1016/S1352-2310(96)00105-7, 1997.

543 Jenkin, M. E., Saunders, S. M., Wagner, V. and Pilling, M. J.: Protocol for the development of
544 the Master Chemical Mechanism, MCM v3 (Part B): tropospheric degradation of aromatic
545 volatile organic compounds, Atmos Chem Phys, 3(1), 181–193, doi:10.5194/acp-3-181-2003,
546 2003.

547 Jenkin, M. E., Young, J. C. and Rickard, A. R.: The MCM v3.3 degradation scheme for
548 isoprene, Atmos Chem Phys Discuss, 15(6), 9709–9766, doi:10.5194/acpd-15-9709-2015,
549 2015.

550 Metzger, A., Dommen, J., Gaeggeler, K., Duplissy, J., Prevot, A. S. H., Kleffmann, J.,
551 Elshorbany, Y., Wisthaler, A. and Baltensperger, U.: Evaluation of 1,3,5 trimethylbenzene
552 degradation in the detailed tropospheric chemistry mechanism, MCMv3.1, using
553 environmental chamber data, Atmos Chem Phys, 8(21), 6453–6468, doi:10.5194/acp-8-6453-
554 2008, 2008.

555 Müller, M., George, C. and D'Anna, B.: Enhanced spectral analysis of C-TOF Aerosol Mass
556 Spectrometer data: Iterative residual analysis and cumulative peak fitting, Int. J. Mass

557 Spectrom., 306(1), 1–8, doi:10.1016/j.ijms.2011.04.007, 2011.

558 Müller, M., Mikoviny, T., Jud, W., D'Anna, B. and Wisthaler, A.: A new software tool for the
559 analysis of high resolution PTR-TOF mass spectra, Chemom. Intell. Lab. Syst., 127, 158–165,
560 doi:10.1016/j.chemolab.2013.06.011, 2013.

561 Müller, M., Mikoviny, T., Feil, S., Haidacher, S., Hanel, G., Hartungen, E., Jordan, A., Märk,
562 L., Mutschlechner, P., Schottkowsky, R., Sulzer, P., Crawford, J. H. and Wisthaler, A.: A
563 compact PTR-ToF-MS instrument for airborne measurements of volatile organic compounds
564 at high spatiotemporal resolution, Atmos Meas Tech, 7(11), 3763–3772, doi:10.5194/amt-7-
565 3763-2014, 2014.

566 Randerson, J. T., Chen, Y., van der Werf, G. R., Rogers, B. M. and Morton, D. C.: Global
567 burned area and biomass burning emissions from small fires, J. Geophys. Res., 117, G04012,
568 doi:10.1029/2012JG002128, 2012.

569 Ridley, B. A. and Grahek, F. E.: A Small, Low Flow, High Sensitivity Reaction Vessel for
570 NO Chemiluminescence Detectors, J. Atmospheric Ocean. Technol., 7(2), 307–311,
571 doi:10.1175/1520-0426(1990)007<0307:ASLFHS>2.0.CO;2, 1990.

572 Sachse, G. W., Hill, G. F., Wade, L. O. and Perry, M. G.: Fast-response, high-precision
573 carbon monoxide sensor using a tunable diode laser absorption technique, J. Geophys. Res.,
574 92, 2071–2081, doi:10.1029/JD092iD02p02071, 1987.

575 Saunders, S. M., Jenkin, M. E., Derwent, R. G. and Pilling, M. J.: Protocol for the
576 development of the Master Chemical Mechanism, MCM v3 (Part A): tropospheric
577 degradation of non-aromatic volatile organic compounds, Atmos Chem Phys, 3(1), 161–180,
578 doi:10.5194/acp-3-161-2003, 2003.

579 Simoneit, B. R. T.: Biomass burning — a review of organic tracers for smoke from
580 incomplete combustion, Appl. Geochem., 17(3), 129–162, doi:10.1016/S0883-
581 2927(01)00061-0, 2002.

582 Stockwell, C. E., Veres, P. R., Williams, J. and Yokelson, R. J.: Characterization of biomass
583 burning emissions from cooking fires, peat, crop residue, and other fuels with high-resolution
584 proton-transfer-reaction time-of-flight mass spectrometry, Atmos Chem Phys, 15(2), 845–
585 865, doi:10.5194/acp-15-845-2015, 2015.

586 Vay, S. A., Choi, Y., Vadrevu, K. P., Blake, D. R., Tyler, S. C., Wisthaler, A., Hecobian, A.,

587 Kondo, Y., Diskin, G. S., Sachse, G. W., Woo, J.-H., Weinheimer, A. J., Burkhart, J. F.,
588 Stohl, A. and Wennberg, P. O.: Patterns of CO2 and radiocarbon across high northern
589 latitudes during International Polar Year 2008, J. Geophys. Res. Atmospheres, 116(D14),
590 D14301, doi:10.1029/2011JD015643, 2011.

591 Veres, P., Roberts, J. M., Burling, I. R., Warneke, C., de Gouw, J. and Yokelson, R. J.:
592 Measurements of gas-phase inorganic and organic acids from biomass fires by negative-ion
593 proton-transfer chemical-ionization mass spectrometry, J. Geophys. Res. Atmospheres,
594 115(D23), D23302, doi:10.1029/2010JD014033, 2010.

595 Warneke, C., Roberts, J. M., Veres, P., Gilman, J., Kuster, W. C., Burling, I., Yokelson, R.
596 and de Gouw, J. A.: VOC identification and inter-comparison from laboratory biomass
597 burning using PTR-MS and PIT-MS, Int. J. Mass Spectrom., 303(1), 6–14,
598 doi:10.1016/j.ijms.2010.12.002, 2011.

599 Weibring, P., Richter, D., Walega, J. G. and Fried, A.: First demonstration of a high
600 performance difference frequency spectrometer on airborne platforms, Opt. Express, 15(21),
601 13476, doi:10.1364/OE.15.013476, 2007.

602 Wisthaler, A., Hansel, A., Kleffmann, J., Brauers, T., Rohrer, F. and Wahner, A.: Real-time
603 detection of nitrous acid (HONO) by PTR-MS a comparison with LOPAP measurements in
604 the atmosphere simulation chamber SAPHIR, p. 402. [online] Available from:
605 http://adsabs.harvard.edu/abs/2003EAEJA.....402W (Accessed 3 September 2015), 2003.

606 Wolfe, G. M. and Thornton, J. A.: The Chemistry of Atmosphere-Forest Exchange (CAFE)
607 Model – Part 1: Model description and characterization, Atmos Chem Phys, 11(1), 77–101,
608 doi:10.5194/acp-11-77-2011, 2011.

609 Wolfe, G., Thornton, J., Merrill, W., Overview of the UW Chemical Model, User Guide -
610 Version 2.1, last updated 10/12/2012

611 Yokelson, R. J., Griffith, D. W. T. and Ward, D. E.: Open-path Fourier transform infrared
612 studies of large-scale laboratory biomass fires, J. Geophys. Res. Atmospheres, 101(D15),
613 21067–21080, doi:10.1029/96JD01800, 1996.

614 Yokelson, R. J., Goode, J. G., Ward, D. E., Susott, R. A., Babbitt, R. E., Wade, D. D.,
615 Bertschi, I., Griffith, D. W. T. and Hao, W. M.: Emissions of formaldehyde, acetic acid,
616 methanol, and other trace gases from biomass fires in North Carolina measured by airborne

Formatted: Widow/Orphan control, Adjust space between Latin and Asian text, Adjust space between Asian text and numbers

Formatted: Font color: Black

617 Fourier transform infrared spectroscopy, J. Geophys. Res. Atmospheres, 104(D23), 30109–
618 30125, doi:10.1029/1999JD900817, 1999.

619 Yokelson, R. J., Crounse, J. D., DeCarlo, P. F., Karl, T., Urbanski, S., Atlas, E., Campos, T.,
620 Shinozuka, Y., Kapustin, V., Clarke, A. D., Weinheimer, A., Knapp, D. J., Montzka, D. D.,
621 Holloway, J., Weibring, P., Flocke, F., Zheng, W., Toohey, D., Wennberg, P. O.,
622 Wiedinmyer, C., Mauldin, L., Fried, A., Richter, D., Walega, J., Jimenez, J. L., Adachi, K.,
623 Buseck, P. R., Hall, S. R. and Shetter, R.: Emissions from biomass burning in the Yucatan,
624 Atmos Chem Phys, 9(15), 5785–5812, doi:10.5194/acp-9-5785-2009, 2009.

625 Yokelson, R. J., Burling, I. R., Gilman, J. B., Warneke, C., Stockwell, C. E., de Gouw, J.,
626 Akagi, S. K., Urbanski, S. P., Veres, P., Roberts, J. M., Kuster, W. C., Reardon, J., Griffith,
627 D. W. T., Johnson, T. J., Hosseini, S., Miller, J. W., Cocker III, D. R., Jung, H. and Weise, D.
628 R.: Coupling field and laboratory measurements to estimate the emission factors of identified
629 and unidentified trace gases for prescribed fires, Atmos Chem Phys, 13(1), 89–116,
630 doi:10.5194/acp-13-89-2013, 2013.

631